Numerical investigation of non-Newtonian inelastic flows through conical nozzles

Ahmed M shareef[1]   **Alaa H. Al-Muslimawi[2]**

ahmad.muhamad.sci@uobasrah.edu.iq   alaa.abdullah@uobasrah.edu.iq

[1]   Department of Mathematics, College of Science, University of Basrah, Basrah, Iraq
[2] Department of Mathematics, College of Science, University of Basrah, Basrah, Iraq

Abstract

The numerical analysis for the incompressible power-low inelastic fluid is described in this work. To characterize the fluid's motion, a mass conservation equation and momentum conservation equation are used. The investigation was carried out numerically using a Taylor Galerkin-pressure correction (TG-PC) method. The contrast of Newtonian findings with shear-thinning inelastic is highlighted. The convergence of solution components is examined under the variation of Reynolds number (*Re*) and the parameters of power-low inelastic model (PLIM). The results show that the inelastic factors have a considerable influence on the level of temporal convergence rates of velocity, while there is minor change in the level of pressure convergence.

Keywords: Conical nozzles; Galerkin method; General Newtonian; Power-law model; Viscosity.

Journal of Education for Pure Science- University of Thi-Qar
Vol.13, No.4 (Dec2023)
Website: jceps.utq.edu.iq   *Email: jceps@eps.utq.edu.iq*

1. Introduction:

The conical nozzles play an important role in the modern industrial process field, such as the automotive industry and the aerospace industry, due to their great role in controlling the flow of liquids and gases. This procedure requires that providing a pointed hole through, which the material passes [1], and then achieve optimal results, such as controlling and increasing thrust in the speed and direction of fluid flow. Experts improved performance and efficiency in various operations through the distinctive shape of the conical nozzle [2,3]. This shape also contributed to improving control over pressure distribution and reducing turbulence and pressure losses. Therefore, conical nozzles are important tools that contribute to technological progress across multiple fields [1]. Schmidt et al. [6] (1997) studied the he effects of several nozzle parameters on cavitating nozzle flow by employing a two-dimensional transient model. The effect of many factors on the flow characteristics, such as the cone's half-angle, the ratio of hole's length to diameter, and the ratio of the upstream diameter to the downstream diameter has studied by Wang et al. [8] (2019). Due to this importance, many studies have been conducted on this type of flow. Nair et al. [3] (2019) studied the rocket nozzles through using truncated conical plug nozzle and Conical plug nozzle. The numerical simulation for the flow through these plug nozzles is conducted and compared the results with experimental data. Singh et al. [4] (2019) are developed the reference to obtain an optimal structure for nozzle geometry, where the critical pressure ratio is increased while minimizing pressure drop across the nozzle. Moreover, improvement the behaviors of dynamical flow of a compound droplet moving in a nozzle with a conical shape in the downstream region via front tracking-based simulations is investigated by Truong et al. [5] (2020). Ahmed and Al-Muslimawi [6] (2020) developed a numerical method based on the Galerkin finite element method to study the incompressible Newtonian laminar flow through a conical channel.

Numerically, a Taylor Galerkin-pressure correction (TG-PC) method is employed in this study to treat the governing equations. This approach is presented by Townsend and Webster [7] to traet Newtonian and non-Newtonian fluid flows high accuracy. Essentially, this method is resulted from combines a pressure correction method with the Taylor Galerkin method, which contributes to improving efficiency and accuracy in solving all complex fluid flow problems. The TG-PC-method is presented based on time incremental method, which is essentially known as a two-step Lax-Wendroff. The pressure-correction technique considers the incompressibility limitation to ensure second-order accuracy in time (for more details see [8-12]) .

In the present study, the incompressible Navier-Stokes equations in axisymmetric cylindrical coordinates are introduced. Navier-Stokes equations represent the governing equation of the fluid flow phenomena.

These equations consist of the conversation of mass and momentum equations. In addition, we concern in this study on inelastic conical nozzles fluid flow in both shear-thickening and shear-thinning situations. The viscosity of an inelastic fluid is represented by the simplest basic constitutive equation, which uses a power law model to express the behavior of shear thinning and shear thickening in fluids. Ostwald–de Waele suggested this model and it is dependent on shear rat and represent by the following form [13]:

$$\mu_s = k(\dot{\gamma})^{n-1},$$

where *n* is the power law index and *k* is the consistency parameter. Here, a more viscous fluid is indicated by higher *k* values. In the case of *n* values equal to 1 the fluid is Newtonian, but when *n is* less than 1, shear thinning is observed. In the case of *n* greater than 1, shear thickness is also observed [14]. Thus, many chemical and industrial fluids are dealt with by this model. The current work focuses on a variety of physical factors such as the consistency (*k*), Reynolds number (*Re*) and power law index (*n*) to examine the flow properties of the power law liquids. The effect of these factors on fluid behavior has been studied in this research.

The following is how this paper is organized: inelastic isothermal flow motion is mathematically modeled in Section 2, along with instructions on how to translate the modeling into a non-dimensional format. We present the numerical methodology (TG-PC) and the relevant finite element technique features in Section 3. Sections 4 and 5 give the problem specification and the numerical findings associated with it, respectively.

2. Mathematical modeling

The mathematical differential equations of incompressible isothermal inelastic flow when body forces are ignored can be written as:

$$\nabla \cdot u = 0, \tag{1}$$

$$\rho \frac{\partial u}{\partial t} = \nabla \cdot (2\mu_s(\dot{\gamma}, \dot{\varepsilon})d) - \rho u \cdot \nabla u - \nabla p. \tag{2}$$

Here, the symbols for velocity, density, hydrodynamic pressure, and solvent viscosity are u, ρ, p, and μ_s, respectively. Furthermore, ∇ and $d = \frac{1}{2}(\nabla u + \nabla u^\tau)$ represent the gradient operator and the rate of the deformation tensor. In addition, the shear rate $(\dot{\gamma})$ and strain rate $(\dot{\varepsilon})$ are defined as:

$$\begin{aligned} \dot{\gamma} &= 2\sqrt{II_d} \\ \dot{\varepsilon} &= 3\frac{III_d}{II_d} \end{aligned}, \tag{3}$$

where, II_d and III_d stand for the second and third invariants of the rate of strain tensor d. [13]:

$$II_d = \frac{1}{2}\text{tr}(d^2) = \frac{1}{2}\left\{\left(\frac{\partial u_r}{\partial r}\right)^2 + \left(\frac{\partial u_z}{\partial z}\right)^2 + \left(\frac{u_r}{r}\right)^2 + \frac{1}{2}\left(\frac{\partial u_r}{\partial z} + \frac{\partial u_z}{\partial r}\right)^2\right\}. \tag{4}$$

Journal of Education for Pure Science- University of Thi-Qar
Vol.13, No.4 (Dec2023)
Website: jceps.utq.edu.iq   *Email: jceps@eps.utq.edu.iq*

And

$$III_d = \det(d) = \frac{u_r}{r}\left\{\frac{\partial u_r}{\partial r}\frac{\partial u_z}{\partial z} - \frac{1}{4}\left(\frac{\partial u_r}{\partial z} + \frac{\partial u_z}{\partial r}\right)^2\right\}. \tag{5}$$

Furthermore, the constitutive formula (Power Law Equation) is

$$\mu_s = k(\dot{\gamma})^{n-1}, \tag{6}$$

where the power-law index is denoted by *n* and the consistency parameter by *k*.

By utilizing the scaling $Re = \rho\frac{UL}{\mu}$, on the other hand, the equation may also be expressed in terms of the non-dimensional groups of Reynolds numbers (Re), with (ρ), (L), and (U) standing for the characteristic density lengths and velocities, respectively[15].Therefore, the non-dimensional form of equation 2 is given as:

$$Re\left(\frac{\partial v}{\partial t} + u \cdot \nabla u\right) = -\nabla p + \nabla \cdot (2\mu_s(\dot{\gamma},\dot{\varepsilon})d). \tag{7}$$

3. Numerical method and boundary conditions

The (TG-PC) method is used in the present investigation. This approach consists of three basic stages. In the first phase, a two-step predictor-corrector technique is utilized to compute the u^* components by providing the initial velocity and pressure fields. The Choleski technique is utilized to calculate the pressure differences during the second phase $(P^{n+1} - P^n)$ based on u^* [14-17]. Finally, the velocity field u^{n+1} is evaluated when, u^* and pressure difference $(P^{n+1} - P^n)$ are adopted by employing the Jacobi iteration [15,21]. Then these fractional stages can be written as

Stage1a: $\frac{2Re}{\Delta t}\left[u^{n+\frac{1}{2}} - u^n\right] = L(u^n, d^n) - \nabla p^n,$ (9)

Stage1b: $\frac{Re}{\Delta t}[u^* - u^n] = L\left(u^{n+\frac{1}{2}}, d^{n+\frac{1}{2}}\right) - \nabla p^n,$ (10)

Stage2: $\nabla^2(p^{n+1} - p^n) = \frac{Re}{\theta\Delta t}\nabla \cdot u^*,$ (11)

Stage3: $u^{n+1} = u^* - \frac{\theta\Delta t}{Re}[\nabla(p^{n+1} - p^n)].$ (12)

Where,

$$L(u, d) = [\nabla \cdot (2\mu_s(\dot{\gamma},\dot{\varepsilon})d) - Re\, u \cdot \nabla u]. \tag{13}$$

Also, $\theta \in [0,1]$, if choosing $\theta = 1/2$ is chosen, the following technique is popular: the Crank–Nicolson scheme and is referred to as the Crank–Nicolson parameter, [16-18].

The approximate form of velocity and pressure is presented as:

$$u(x,t) = \sum_{j=1}^{Ju} u_j(t)\phi_j(x), \tag{14}$$

$$p(x,t) = \sum_{j=1}^{Jp} p_j(t)\psi_j(x), \tag{15}\text{where, } J_u$$

Journal of Education for Pure Science- University of Thi-Qar
Vol.13, No.4 (Dec2023)
Website: jceps.utq.edu.iq   *Email: jceps@eps.utq.edu.iq*

represents the total number of nodes, and J_p is the number of vertices of triangles. $u_j(t)$ and $p_j(t)$ are the vector of velocity and pressure nodal values. $\phi_j(x)$ and $\psi_j(x)$ are the functions that form their basis (shape or interpolation) such that $\phi_j(x)$ are chosen as the quadratic basis function and $\psi_j(x)$ as a linear. The pressure is presented at the mid-side nodes, in contrast the velocity is evaluated and vertex nodes of a triangular [19]. After the analysis of finite element method, Equations (9), (10), (11), and (12) can be written in matrix form as follows [23,24].

$$\text{Step1a:}\left[\frac{2Re}{\Delta t}M + \frac{1}{2}S\right]\left(U^{n+\frac{1}{2}} - U^n\right) = \{-[S + Re\, N(U)]U + \square^T P\}^n, \tag{16}$$

$$\text{Step 1b: }\left[\frac{Re}{\Delta t}M + \frac{1}{2}S\right](U^* - U^n) = \{-SU + \square^T P\}^n - Re[N(U)U]^{n+\frac{1}{2}}, \tag{17}$$

$$\text{Step2: } K(P^{n+1} - P^n) = -\frac{Re}{\theta\Delta t}\square U^*, \tag{18}$$

$$\text{Step3: }\frac{Re}{\Delta t}M(U^{n+1} - U^*) = \theta\square^T(P^{n+1} - P^n), \tag{19}$$

where, U^n, U^{n+1} and P^n, P^{n+1} are nodal vectors of velocity and pressure at the time t^n and t^{n+1}, respectively; and U^* is an intermediate nodal velocity vector introduced in Step 1b. M, S, N, $\square$, and K respectively represent mass, momentum diffusion, convective, divergence/pressure gradient, and pressure stiffness matrices, [20-26].

Boundary conditions (*BCs*): A schematic flow diagram of the conical nozzle is presented in Figure 1, with the following setting of boundary conditions:

(a) At the inlet, zero radial velocity is applied with axial velocity as Poiseuille (*Ps*) flow.

(b) No-slip BCs on the top wall of the channel, while slip axial velocity (u_z) is applied through axis of symmetry with zero radial velocity.
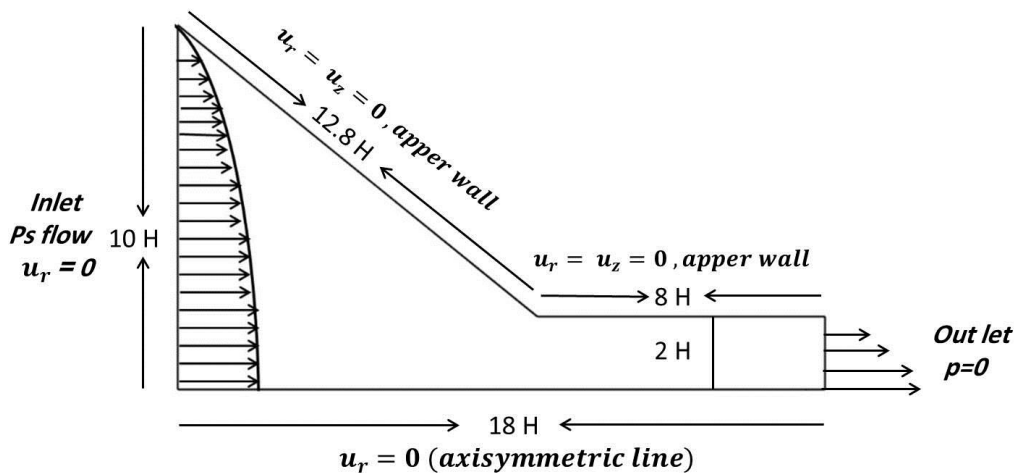
Figure 1 Flow geometry (symmetrical axis).

Journal of Education for Pure Science- University of Thi-Qar
Vol.13, No.4 (Dec2023)
Website: jceps.utq.edu.iq   *Email: jceps@eps.utq.edu.iq*

The effect of k on the convergence rate for axial velocity and pressure is appeared in Figure 2 and 3 for both shear thinning (n=0.8) and shear thickening (n=1.6) with constant Re=5. For shear thinning issue one can see that, by increasing the level of k, less effort and time-steps are needed to reach a specified tolerance level (10^{-6}) for both velocity and pressure, and this is the exactly opposite of what was achieved in the case of shear thickening. In addition, in the shear thickening case we need less time steps to get the monotonic convergence (around 30 time-step) compared to the shear thinning case (around 45 time-step) [1], [10].
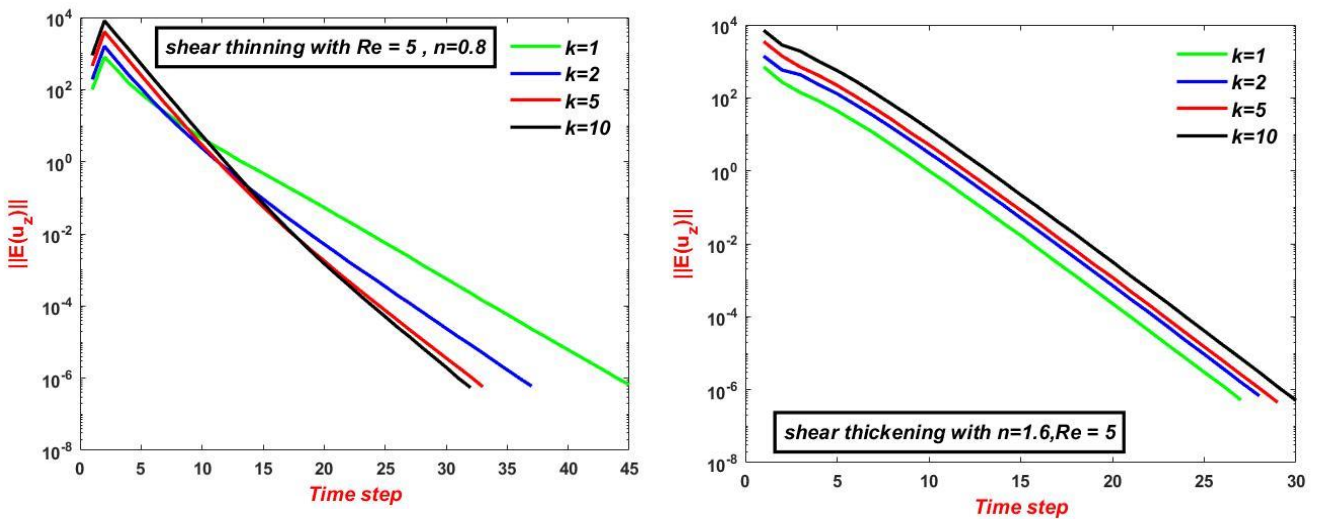
Figure 2 Convergence of velocity, (a) shear thinning, (b) shear thickening; Re=5, k variation.
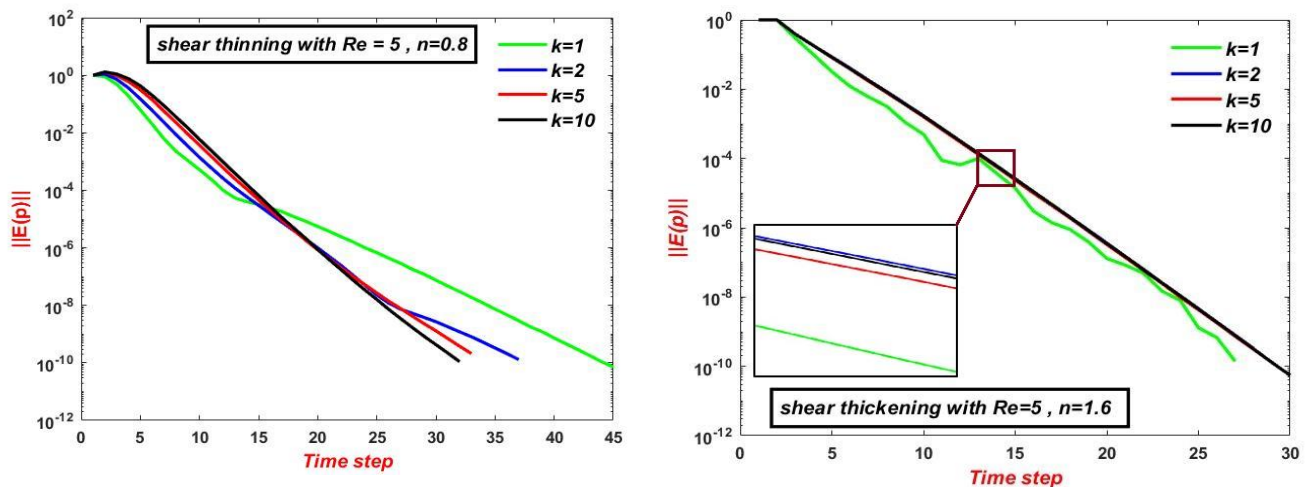
Figure 3 Convergence of pressure, (a) shear thinning, (b) shear thickening; Re=5, k variation.

Journal of Education for Pure Science- University of Thi-Qar
Vol.13, No.4 (Dec2023)
Website: jceps.utq.edu.iq   *Email: jceps@eps.utq.edu.iq*

On the other hand, there was focus on the effect of *Re*-variation on the convergence of velocity and pressure again for shear thinning and shear thickening at fixed *k*=2. Figure 4 and 5 show that, through temporal convergence history tolerances for velocity and pressure one can observed that the level of time-step rises as *Re* increases, with almost same level in both situations shear thickening and shear thinning [1], [10].
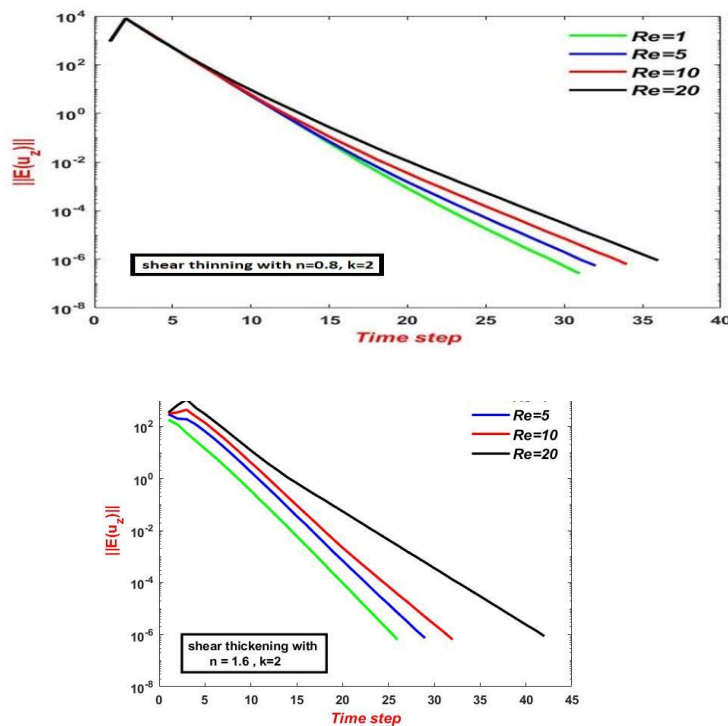
Figure 4 The level of velocity convergence, (a) shear thinning, (b) shear thickening; *k*=2, *Re* variation.
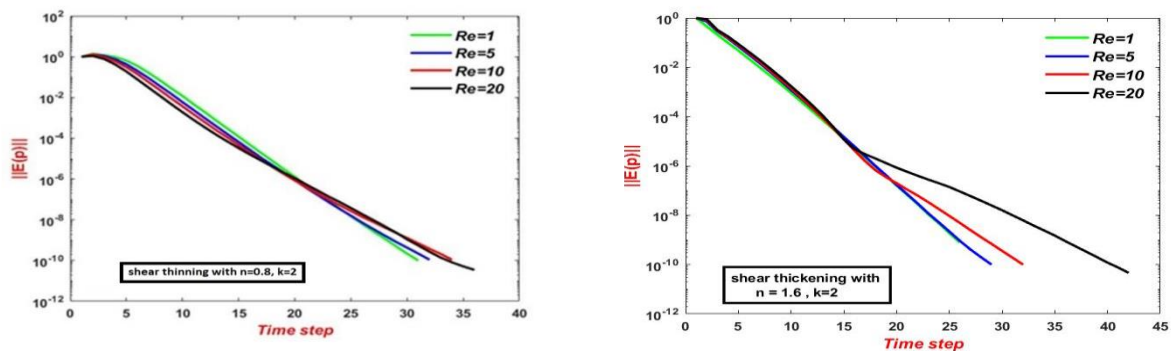
Figure 5 The level of pressure convergence, (a) shear thinning, (b) shear thickening; *k*=2, *Re* variation.

Journal of Education for Pure Science- University of Thi-Qar
Vol.13, No.4 (Dec2023)
Website: jceps.utq.edu.iq   *Email: jceps@eps.utq.edu.iq*

Figure 6 provides the corresponding results for maximum velocity and maximum pressure as a function of n for $Re=1$ and $k=2$. In both components we observed that the levels of velocity and pressure are increased under n increase to reach to the high levels in shear thickening situation which gives a clear feature about the difficulties of convergence for large Re. From the profiles, the maximum level of velocity is occurred in shear thickening area with around 61.5783 units at $n=2$, in the same time the maximum level of pressure also appeared in the shear thickening region. These results are consistent with the physical properties of fluids, as decreasing the value of n leads to an increase in viscosity and greater non-objection to the movement of the fluid, which leads to an increase in the velocity and pressure [6]. More details of the maximum level of components are presented in Table 1.

Table1 max u, max p with n variation.

n	Max u	Max p
0.2	33.5562	500.404
0.3	32.4153	542.379
0.4	33.0627	602.934
0.5	35.2473	684.397
0.6	37.7869	790.441
0.7	40.614	927.68
0.8	43.5901	1104.63
0.9	46.4675	1334.08
1	48.9346	1636.99
1.1	50.8341	2046.22
1.2	52.344	2611.82
1.3	53.6186	3406.47
1.4	54.8793	4532.61
1.5	56.1489	6135.28
1.6	57.3045	8422.21
1.7	58.3201	11691.5
1.8	59.3441	15672.3
1.9	60.4002	19341.5
2	61.5783	23521.8
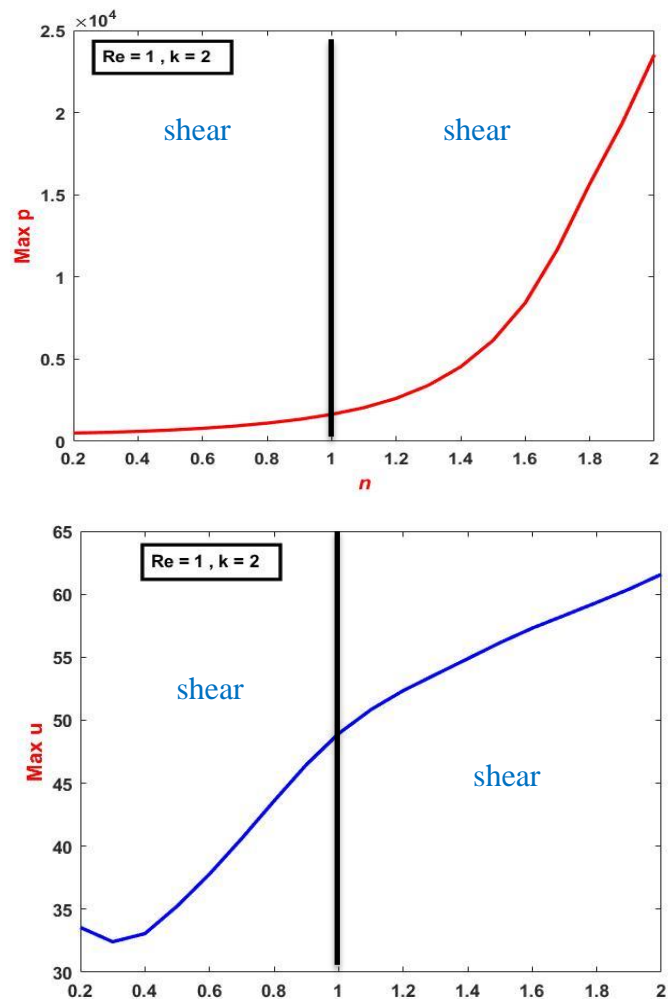
Figure 6. Max velocity and max pressure with $Re = 1$, $k = 2$.

Journal of Education for Pure Science- University of Thi-Qar
Vol.13, No.4 (Dec2023)
Website: jceps.utq.edu.iq   *Email: jceps@eps.utq.edu.iq*

The maximum velocity and pressure are plotted in Figure 7 as a function of k at fixed $Re=1$, and $n=\{0.6, 1.6\}$ under k-variation. In all cases the value of velocity and pressure is increased ask increases, with high level is occurred in the case of shear thickening. For example, from the velocity profiles one can observe increase of almost 26% in shear thickening for $k=20$, whereas the increase in pressure was noticeable, around 96%. In addition, we observed that the increase in velocity takes a non-linear character, unlike that of the pressure, where it was a linear increase. More details of the results are given in Table 2.

(a) shear thinning
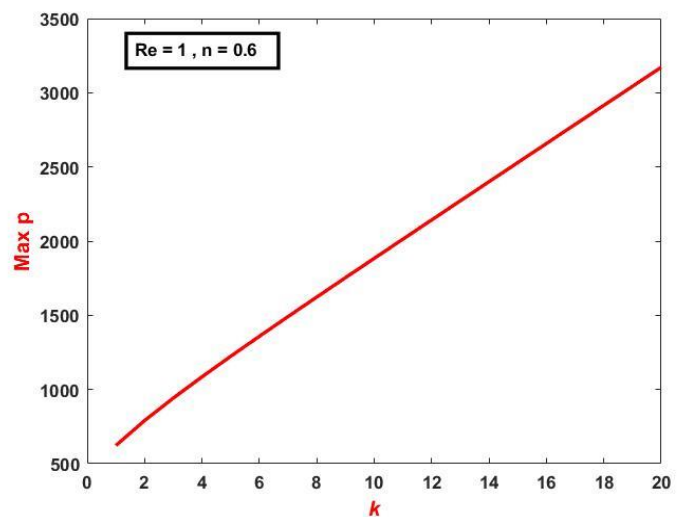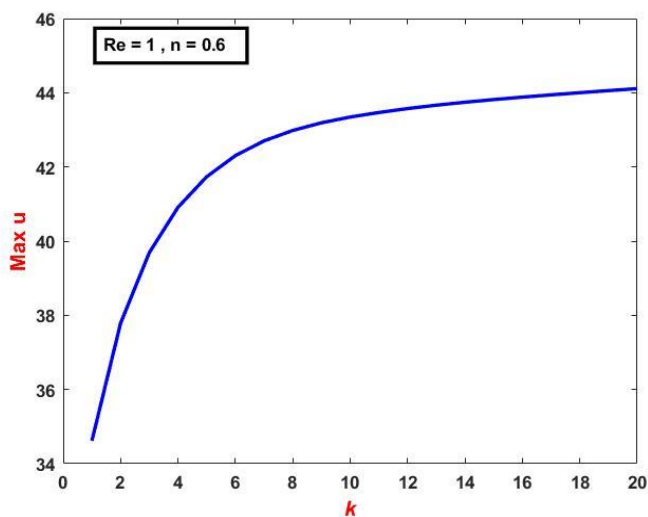
(b) shear thickening
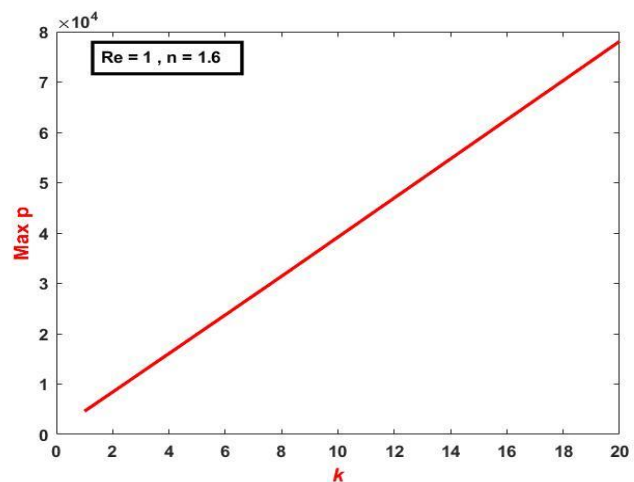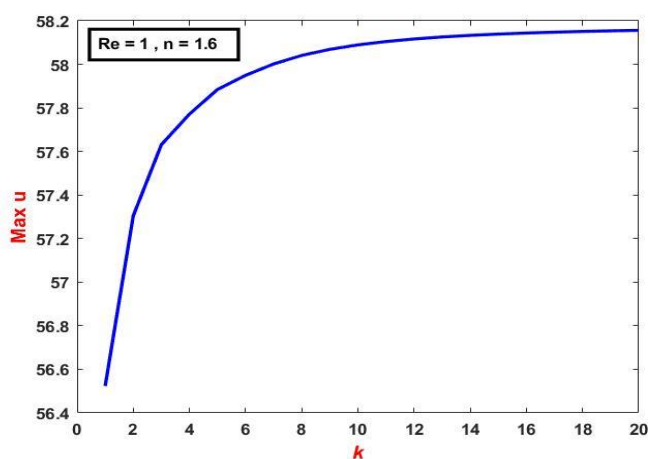
Figure 7 Max velocity and pressure with k-variation, n=0.6, 1.6, Re =1.

Table 2 Max velocity and pressure with *k*-variation, *n*=0.6, *Re* =1.

K	n=0.6		n=1.6	
	Max u	Max p	Max u	Max p
1	34.6162	622.552	56.5233	4611.98
2	37.7869	790.441	57.3045	8422.21
3	39.6891	942.08	57.6309	12244.7
4	40.9118	1085.36	57.7714	16047.2
5	417365	1223.61	57.8845	19907.7
6	42.306	1358.65	57.9493	23743.6
7	42.7026	1491.6	58.0016	27581
8	42.9838	1623.15	58.0408	31422.3
9	43.19	1753.77	58.0686	35307.9
10	43.346	1883.75	58.0891	39194.1
11	43.4674	2013.28	58.1044	43080.8
12	43.5733	2142.5	58.1162	46967.9
13	43.6647	2271.5	58.1255	50855.3
14	43.7441	2400.34	58.1328	54742.9
15	43.8157	2529.06	58.1387	58630.6
16	43.8815	2657.7	58.1435	62518.5
17	43.943	2786.28	58.1475	66406.6
18	44.0013	2914.8	58.1508	70294.7
19	44.0571	3043.3	58.1536	74183
20	44.1109	3171.76	58.156	78071.3

The effect of *Re* number on velocity and pressure are presented in Figure 8 again for shear thinning and shear thickening and fixed *k*=2. Here, the velocity and pressure are plotted as a function of *Re*. The findings show that there are two opposite trends in the results, where we can observe that rise in the pressure with increase in *Re* and a decrease in the velocity with increase in *Re*. In addition, the level of solution is higher in the case of shear thickening [6]. Moreover, the field structures in velocity are displayed in Figure 9 for *n*-variation.

(a) shear thinning
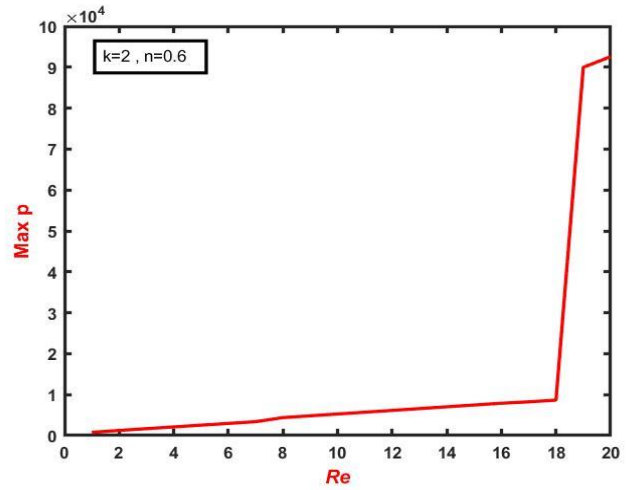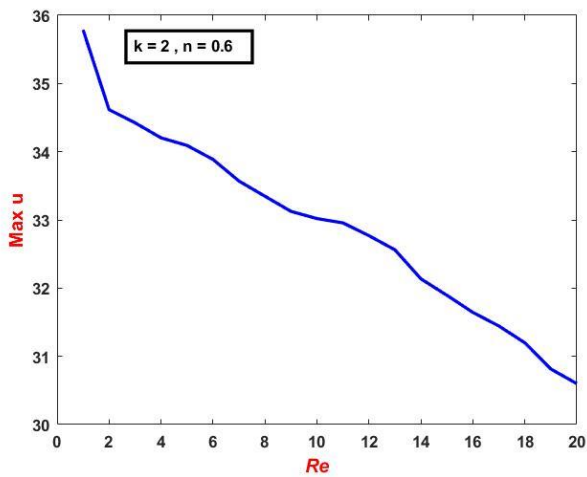
(b) shear thickening
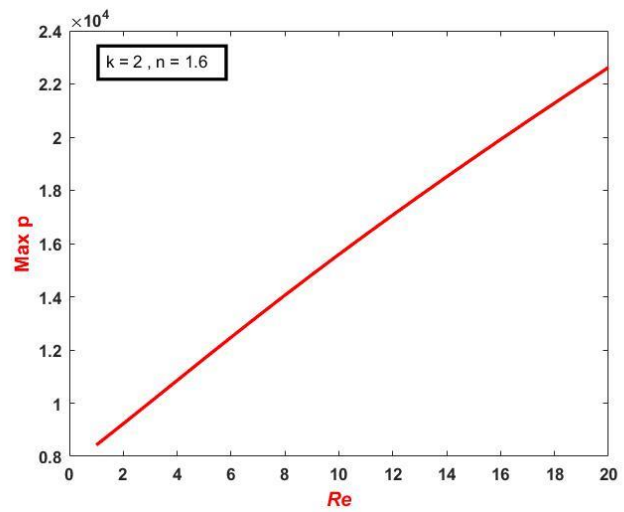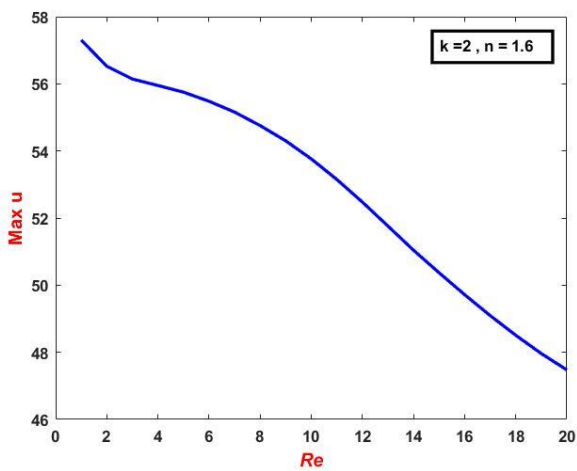
Figure 8 Max velocity and pressure, $n=\{0.6, 1.6\}$, $k=1$; Re-variation.

Journal of Education for Pure Science- University of Thi-Qar
Vol.13, No.4 (Dec2023)
Website: jceps.utq.edu.iq   *Email: jceps@eps.utq.edu.iq*
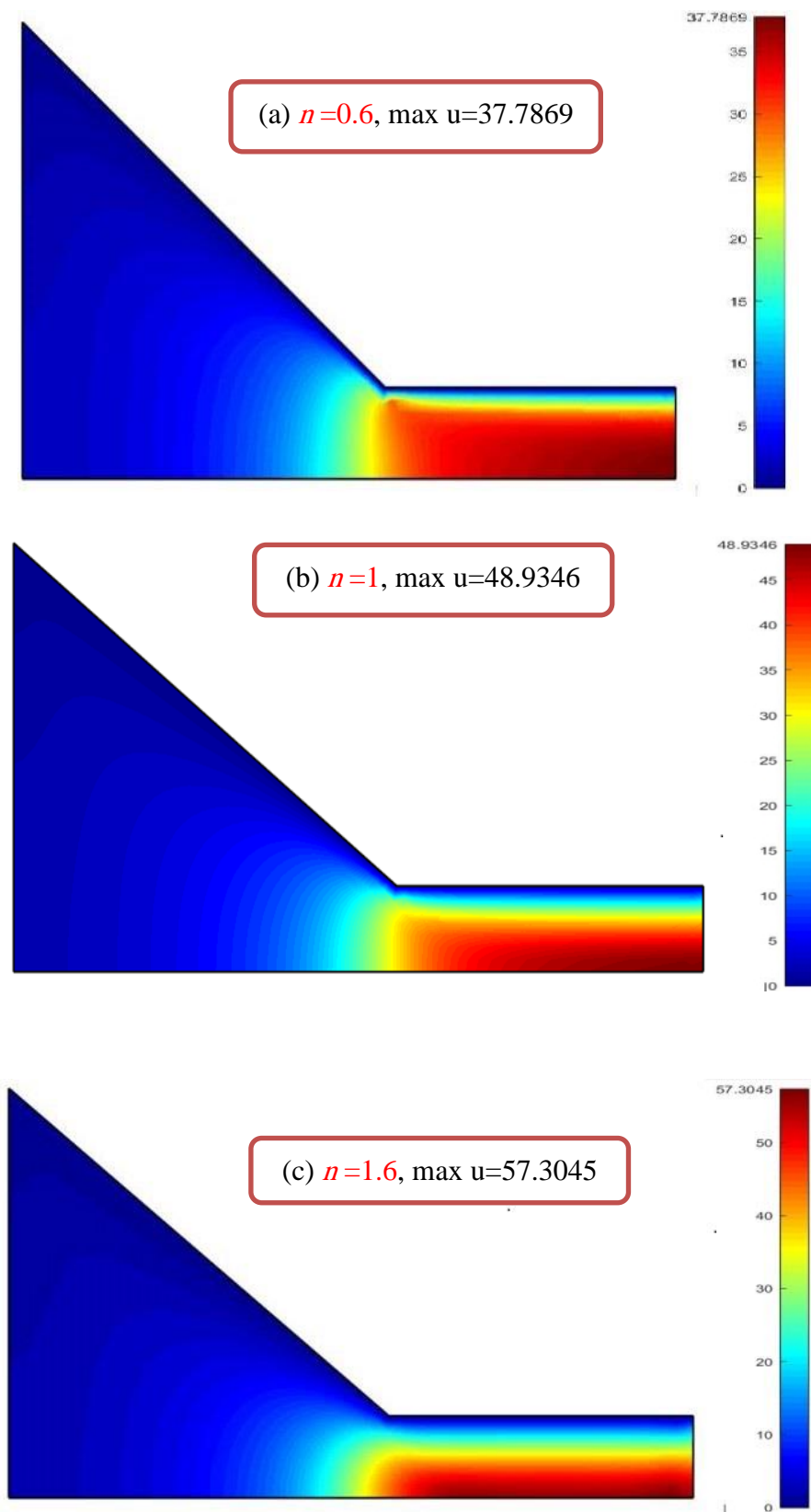
Figure 9 Velocity field; n =0.6, 1, 1.6.

Journal of Education for Pure Science- University of Thi-Qar
Vol.13, No.4 (Dec2023)
Website: jceps.utq.edu.iq   *Email: jceps@eps.utq.edu.iq*

Velocity and pressure drop are plotted in Figure 10 under $n=\{0.6, 1, 1.6\}$, $Re=1$ and $k=2$ over the centerline. The results show that there is a significant impact of n-variation on the velocity and pressure along the channel. In this context, the level of pressure drop decreased as n decreases, reaching a peak of around 8300 units with $n = 1.6$ (see Figure 10b). In contrast, the results of velocity are reflected a same feature of pressure, with maximum level is occurred at the outlet of the conical at n=1.6; of around 58 units (see Figure 10a).

(a)   (b)
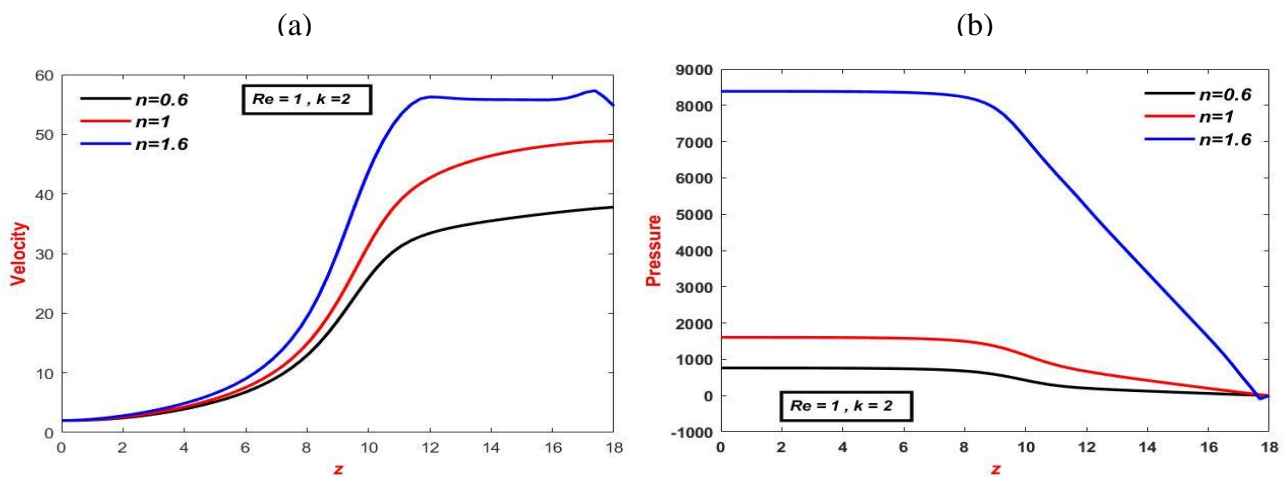
Figure 10 Velocity on symmetric line, pressure in symmetric line, $Re = 1$, $k = 2$.

The profiles of the axial velocity in fully developed flow at different regions z ={0, 3.6, 7.2, 10.8, 14.4, 18} are illustrated in Figure 11 in the shear thinning situation (n=0.8), Re=1 and k=2. The axial velocity profiles show parabolic flow structure for all zones, with obviously increasing in the level of velocity

Journal of Education for Pure Science- University of Thi-Qar
Vol.13, No.4 (Dec2023)
Website: jceps.utq.edu.iq   *Email: jceps@eps.utq.edu.iq*
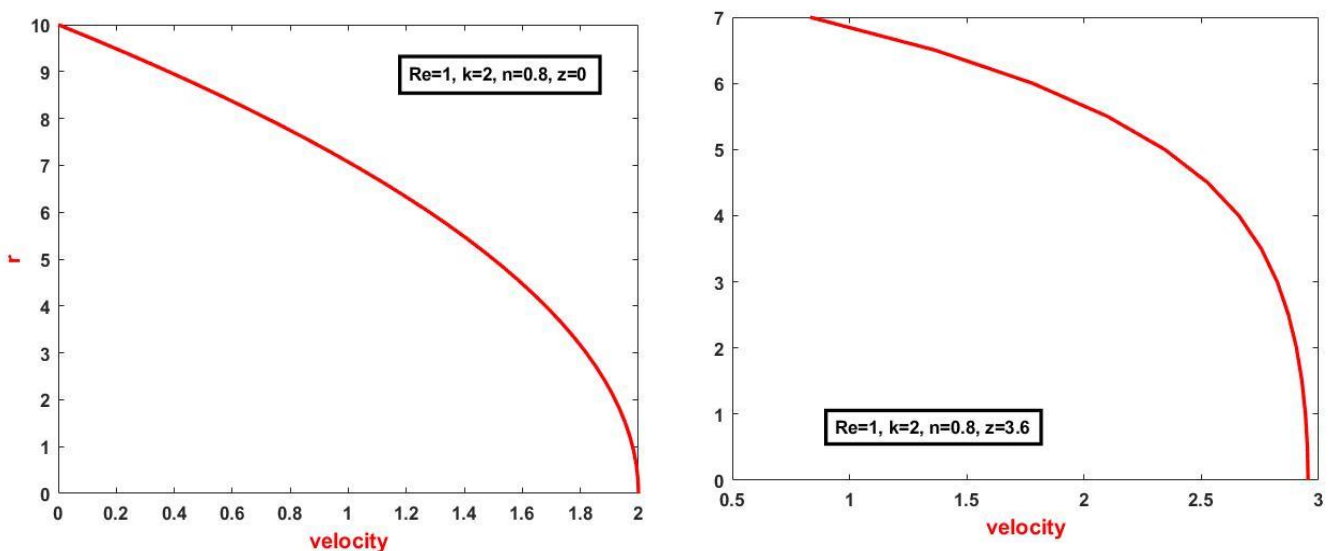
whenever we are trending to the cone exit, approaching to the maxima of units.
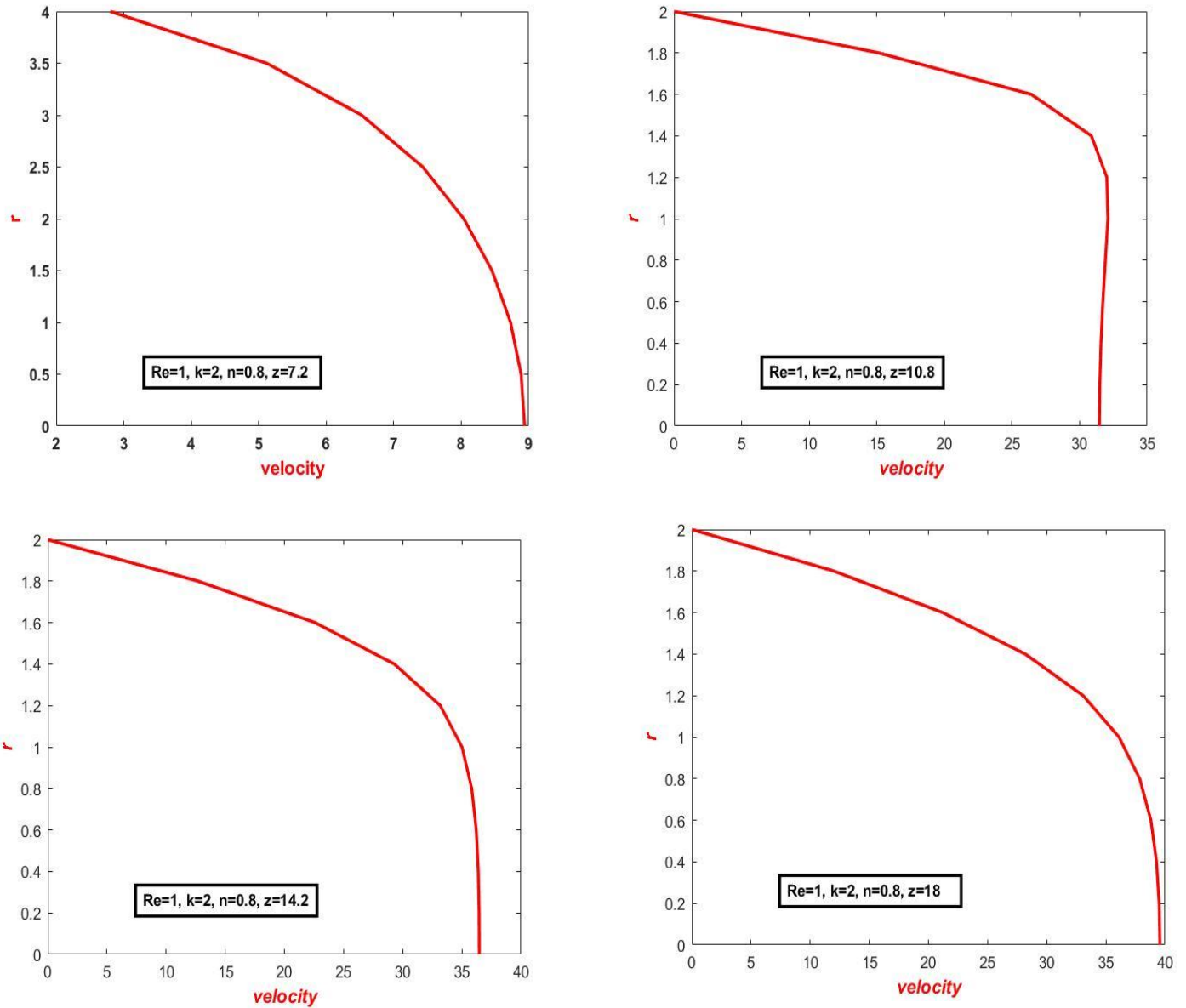
Figure 11 Velocity on symmetric line, at z={0, 3.6, 7.2, 10.8, 14.4, 18}.

Conclusions

In the cylindrical coordinates system, the (TG-PC)-method is used to model incompressible inelastic conical nozzles flows. The primary goals of this research are to determine the influence of the Reynolds number (Re), consistency parameter (k) and power law index (n) on the amount of convergence in shear thickening and shear thinning scenarios. Furthermore, the crucial Re for both flow scenarios is examined. In both situations of shear thinning and shear thickening, the convergence level of pressure and velocity rises as the power-law index (n) grows. Furthermore, the convergence rate in shear thickening flow is greater than that in shear thinning flow. The same characteristic is found for Re-variation and k-variation. Additionally, shear thinning and shear thickening were once again the main focus of the influence of contrast on velocity and stress convergence. In both shear thickening and shear thinning scenarios, we have shown that the level of the time step rises with increased renewable energy through the temporal convergence of the pressure and speed changes.

References

[1] Sharhanl, A. A., & Al-Muslimawi, A. (2021). Numerical simulation of a power-law inelastic fluid in axisymmetric contraction by using a Taylor Galerkin-pressure correction finite element method. International Journal of Nonlinear Analysis and Applications,12(SpecialIssue),2211-2222. https://ijnaa.semnan.ac.ir/article_6113.html

[2] Gresho, P. M., Lee, R. L., Chan, S. T., & Sani, R. L. (1980). Solution of the time-dependent incompressible Navier-Stokes and Boussinesq equations using the Galerkin finite element method. In Approximation Methods for Navier-Stokes Problems: Proceedings of the Symposium Held by the International Union of Theoretical and Applied Mechanics (IUTAM) at the University of Paderborn, Germany, September 9–15,1979 (pp. 203-222). Springer Berlin Heidelberg.https://doi.org/10.1007/BFb00869.

[3] Nair, P. P., Suryan, A., & Kim, H. D. (2019). Computational study on flow through truncated conical plug nozzle with base bleed. Propulsion and Power Research, 8(2), 108-120. https://doi.org/10.1016/j.jppr.2019.02.001

[4] Singh, J., Zerpa, L. E., Partington, B., & Gamboa, J. (2019). Effect of nozzle geometry on critical-subcritical flow transitions. Heliyon, 5(2).
https://doi.org/10.1016/j.heliyon.2019.e01273.

[5] Vu, T. V., Bui, D. T., Nguyen, Q. D., & Pham, P. H. (2020). Numerical study of rheological behaviors of a compound droplet in a conical nozzle. International Journal ofHeat and Fluid Flow, 85, 108655. https://doi.org/10.1016/j.ijheatfluidflow.2020.108655

[6] Yasir, R. Y., & Al-Muslimawi, A. H. (2019). Numerical simulation of Power-Law inelastic fluid in channal by using finite element method. Basrah Journal of Science, 37(2), 163-180. https://doi.org/10.29072/basjs.20190202.

[7]] Townsend, P., and M. F. Webster.(1987) "An Algorithm for the Three-Dimensional Transient Simulation of Non-Newtonian Fluid Flows." Transient/Dynamic Analysis and Constitutive Laws for Engineering Materials, , pp. 123–133. https://doi.org/10.1007/978-94-009-3655-3_12

[8] Al-Muslimawi, A. H. (2018). Taylor Galerkin pressure correction (TGPC) finite element method for incompressible Newtonian cable-coating flows. Journal of Kufa for Mathematics and Computer, 5(2), 14-22. https://doi.org/10.31642/jokmc/2018/050203.

[9] Al-Muslimawi, A., Tamaddon-Jahromi, H. R., & Webster, M. F. (2013). Numerical simulation of tube-tooling cable-coating with polymer melts. Korea-Australia Rheology Journal, 25, 197-216. https://doi.org/10.1007/s13367-013-0021-x.

[10] Yasir, R. Y., Al-Muslimawi, A. H., & Jassim, B. K. (2020). Numerical simulation of non-Newtonian inelastic flows in channel based on artificial compressibility method. Journal of Applied and Computational Mechanics, 6(2), 271-283.2383-4536 jacm.SCU.ac.ir. https://doi.org/10.22055/JACM.2019.29948.1650

[11] Hawken, D. M., Tamaddon- Jahromi, H. R., Townsend, P., & Webster, M. F. (1990). A Taylor–Galerkin- based algorithm for viscous incompressible flow. International Journal for Numerical Methods in Fluids, 10(3), 327-351. https://doi.org/10.1002/fld.1650100307

[12] Hawken, D. M., Townsend, P., & Webster, M. F. (1991). Numerical simulation of viscous flows in channels with a step. Computers & fluids, 20(1), 59-75.https://doi.org/10.1016/0045-7930(91)90027-f

[13] Belblidia, F., Haroon, T., & Webster, M. F. (2009). The Dynamics of Compressible Herschel—Bulkley Fluids in Die-Swell Flows. Damage and Fracture Mechanics: Failure Analysis of Engineering Materials and Structures, 425-434. https://doi.org/10.1007/978-90-481-2669-9_45

[14] Sivakumar, P., Bharti, R. P., & Chhabra, R. P. (2006). Effect of power-law index on critical parameters for power-law flow across an unconfined circular cylinder. Chemical Engineering Science, 61(18), 6035-6046. https://doi.org/10.1016/j.ces.2006.05.031

[15]Chunyan Wang., Jian Liang., & Hua Huo. (2019). Numerical study of effects of geometric parameters on the flow and cavitation characteristics inside conical nozzle of autonomous underwater vehicle. Advances in Mechanical Engineering 2019, Vol. 11(2) 1–12. https://doi.org/10.1177/1687814019828584.

[16] Schmidt, D. P., Rutland, C. J., & Corradini, M. L. (1997). A numerical study of cavitating flow through various nozzle shapes. SAE transactions, 1664-1673. https://doi.org/10.4271/971597 .

[17] Amirante, R., Distaso, E., & Tamburrano, P. (2014). Experimental and numerical analysis of cavitation in hydraulic proportional directional valves. Energy Conversion and Management, 87, 208-219. https://doi.org/10.1016/j.enconman.2014.07.031

[18] Cavadas, A., de Pinho, F. T., & Campos, J. (2007). Numerical investigation of the flow field in confined impinging jets of power law fluids. Métodos Numéricose Computacionais em Engenharia. https://hdl.handle.net/10216/69599.

[19] Chorin, A. J. (1968). Numerical solution of the Navier-Stokes equations. Mathematics of computation, 22(104), 745-762.   https://doi.org/10.1090/s0025-5718-1968-0242392-2.

[20] Donea, J. (1984). A Taylor–Galerkin method for convective transport problems. International Journal for Numerical Methods in Engineering, 20(1), 101-119.

https://doi.org/10.1002/nme.1620200108.

[21] Aboubacar, M., Matallah, H., & Webster, M. F. (2002). Highly elastic solutions for Oldroyd-B and Phan-Thien/Tanner fluids with a finite volume/element method: planar contraction flows. Journal of Non-Newtonian Fluid Mechanics, 103(1), 65-103. https://doi.org/10.1016/s0377-0257(01)00164-1.

[22] Jahromi, H. T., Webster, M. F., & Williams, P. R. (2011). Excess pressure drop and drag calculations for strain-hardening fluids with mild shear-thinning: Contraction and falling sphere problems. Journal of non-Newtonian fluid mechanics, 166(16), 939-950. https://doi.org/10.1016/j.jnnfm.2011.04.009.

[23] López-Aguilar, J. E., Webster, M. F., Al-Muslimawi, A. H. A., Tamaddon-Jahromi, H. R., Williams, R., Hawkins, K., ... & Lewis, K. (2015). A computational extensional rheology study of two biofluid systems. Rheologica Acta, 54, 287-305.

https://doi.org/10.1007/s00397-014-0830-y.

[24] Coelho, P. M., & Pinho, F. T. (2004). Vortex shedding in cylinder flow of shear-thinning fluids. III: Pressure measurements. Journal of non-Newtonian fluid mechanics, 121(1), 55-68.

https://doi.org/10.1016/j.jnnfm.2004.04.004.

[25] Crank, J., & Nicolson, P. (1947, January). A practical method for numerical evaluation of solutions of partial differential equations of the heat-conduction type. In Mathematical proceedings of the Cambridge philosophical society (Vol. 43, No. 1, pp. 50-67). Cambridge University Press.

https://doi.org/10.1017/s0305004100023197.

[26] Wahba, E. M. "Non-Newtonian fluid hammer in elastic circular pipes: Shear-thinning and shear-thickening effects." Journal of Non-Newtonian Fluid Mechanics 198 (2013): 24-30. https://doi.org/10.1016/j.jnnfm.2013.04.007 .